Direct potential fit analysis of the $X^1\Sigma_g^+$ state of Rb_2: Nothing else will do!

Jenning Y. Seto and Robert J. Le Roy[a)]
Guelph-Waterloo Centre for Graduate Work in Chemistry and Biochemistry, University of Waterloo, Waterloo, Ontario N2L 3G1, Canada

Jean Vergès and Claude Amiot[b)]
Laboratoire Aimé Cotton, Bâtiment 505, Campus d'Orsay, 91405 Orsay Cedex, France

(Received 8 May 2000; accepted 23 May 2000)

High resolution *A-X* emission data involving vibrational levels of the ground $X\,^1\Sigma_g^+$ electronic state up to $v''=113$, spanning 99.8% of the potential well, have been acquired for three isotopomers of Rb_2. While a good fit ($\overline{\sigma_f}=1.03$) to the 12 148 transition frequencies (with uncertainties ± 0.001 cm^{-1}) is obtained from an unconstrained combined-isotopomer Dunham-type analysis, it requires a large number (62) of expansion parameters, and the resulting empirical centrifugal distortion constants (CDCs) are unreliable for extrapolation to higher-*J*. Moreover, Dunham expansion fits using constrained theoretical values of the first six CDCs (up to O_v) fail to properly represent the data, as even higher-order CDCs are required. However, a direct fit of these data to an analytical ''modified Lennard-Jones'' potential energy function involving only 16 fitted parameters yields essentially the same quality of fit as did the unconstrained Dunham fit, and should be reliable for extrapolation to arbitrarily high *J*. This potential form incorporates the proper R^{-6} asymptotic behavior of the potential, and is constrained to have the theoretically predicted C_6 dispersion coefficient. Although the dataset involves the three isotopomers $^{85,85}Rb_2$, $^{85,87}Rb_2$, and $^{87,87}Rb_2$, none of the present analyses was able to determine any Born–Oppenheimer breakdown effects. © *2000 American Institute of Physics.* [S0021-9606(00)01932-2]

I. INTRODUCTION

The Rb_2 molecule has been studied since the beginning of the century, and a comprehensive review of spectroscopic studies up to 1990 was presented by one of us a decade ago.[1] In that paper the observation of ground state vibrational levels up to $v''=112$ obtained by recording laser-induced fluorescence with a Fourier transform spectrometer yielding data with an accuracy of ± 0.005 cm^{-1} was reported. A potential energy curve spanning 99.7% of the potential energy well was obtained from those data.

In recent years Rb_2 has figured prominently in applications of the powerful new technique of photoassociation spectroscopy (PAS) of ultracold atoms. Rubidium has been widely used in laser cooling experiments, and was the medium for the first demonstration of a Bose–Einstein condensate in a dilute medium.[2] An accurate knowledge of the ground-state potential energy curve of this system is necessary for an understanding of ultracold collisions and for the determination of the ''scattering length,'' which is an important parameter in the prediction of Bose–Einstein condensation. To model the potential energy curve satisfactorily, it is important to have accurate observations of very highly excited vibrational levels lying as close as possible to the dissociation limit. Using two-color PAS, Tsai *et al.*[3] observed 12 levels lying within 20 GHz of the dissociation limit of $^{85}Rb_2$, and a coupled-states analysis of those results using the potential of Ref. 1 yielded an accurate new ground-state dissociation energy of $\mathcal{D}_e=3993.53(\pm 0.06)$ cm^{-1}. Other applications of the potential curve of Ref. 1 include (i) the prediction of Feshbach resonances in collisions of ultracold Rb atoms,[4] (ii) the calculation of magnetic-dipolar decay-rate constants in Bose–Einstein condensation experiments,[5] (iii) the prediction of binary collision parameters for ultracold mixed-isotope collisions and the prospect of mixed isotope Bose–Einstein condensation,[6] (iv) the calculation of scattering lengths for ultracold collisions of the short-lived radioactive Rb isotopes,[7] and (v) the formation of cold rubidium molecules in a magneto-optical trap.[8]

The work of Ref. 1 was based on a less extensive and less accurate dataset than that obtained here, and shortcomings of the analysis techniques available at that time required the dataset used in the final analysis to be truncated further. In particular, since the then available computer codes for the calculation of centrifugal distortion constants (CDCs) from a given potential[9] would only generate the first four CDCs, several hundred high-J'' lines had to be omitted from the final ''mechanically consistent'' fits with constrained CDC constants. Moreover, the differences between experiment and the vibrational energies calculated from the final potential showed a disturbingly regular oscillatory behavior (see Fig. 7 of Ref. 1), which suggests the presence of some systematic error. In view of the considerable interest in this system, the present work therefore set out to improve our knowledge of the ground state of Rb_2, both by making new, more accurate measurements, and by applying a more sophisticated method of analysis.

In the following, in Sec. II we describe the experimental

a)Electronic mail: leroy@UWaterloo.ca
b)Electronic mail: Claude.Amiot@lac.u-psud.fr

methodology and measurements, while the results obtained using various methods of analysis and our recommended new ground-state potential energy function are presented in Sec. III.

II. EXPERIMENT

As in previous work,[1] Rb_2 molecules were produced in a stainless steel heat pipe oven by heating rubidium metal (99.95% purity from the Aldrich Chemical Company) with 10 Torr of argon as a buffer gas. The temperature was kept at 600 K, where the vapor pressures of Rb and Rb_2 are, respectively, 2.4 and 0.002 Torr.[10] The molecules were then excited with various fixed frequencies from an Ar^+ laser (Spectra-Physics 171-19) and a Kr^+ laser (Coherent Radiation Innova K-3000), both oscillating under multimode conditions, and by a linear single mode dye laser (Coherent Radiation 599-21) operating with DCM or LD700 dyes pumped by an Ar^+ laser. The emission excited in this way consists of transitions from the three systems $C\,^1\Pi_u \rightarrow X\,^1\Sigma_g^+$, $B\,^1\Pi_u \rightarrow X\,^1\Sigma_g^+$, and $A\,^1\Sigma_u^+ \rightarrow X\,^1\Sigma_g^+$.

As with all other homo- and heteronuclear alkali diatomics, the best way to obtain fluorescence into the highest vibrational levels of the ground state of Rb_2 is to pump the upper levels of the first excited $^1\Sigma_u^+$ electronic state. In particular, due to the relative positions of their potential minima, the best way to obtain spectra nearly up to the dissociation limit of the ground $X\,^1\Sigma_g^+$ state Rb_2 is through the excitation of the $A\,^1\Sigma_u^+$ state. In the present work, isolated $A\,^1\Sigma_u^+ \leftarrow X\,^1\Sigma_g^+$ rovibrational transitions were excited by a cw single frequency titanium sapphire laser (Coherent 899-21) pumped by an argon–ion laser (Spectra Physics 2080-155, all lines power: 18 W). The Ti:Sa laser was operated with the shorter- to the longer-wavelength optics, so its emission range extended from 750 to 1000 nm, with the maximum delivered laser power being 2.3 W.

The experimental arrangement was similar to that described in Ref. 1: backward fluorescence from the heat pipe was collected and focused on the entrance iris of the Fourier transform spectrometer constructed in the Laboratoire Aimé Cotton. The frequency and intensity stability of the lasers was sufficient to allow spectra recording times of about two hours. The wave numbers were calibrated relative to the fixed frequency reference line (the Xe atomic transition near 3.5 μm) used to monitor the path difference of the interferometer. Spectra were recorded between 5 000 and 13 000 cm^{-1} with a resolution limit ranging from 0.005 to 0.012 cm^{-1}, corresponding to the range of Doppler widths in the spectral range studied. The absolute wave number measurement uncertainty varied from 1×10^{-3} cm^{-1} for the strongest lines to 3×10^{-3} cm^{-1} for the weakest ones; these uncertainties are some 3–5 times smaller than those of Ref. 1.

A typical $A\,^1\Sigma_u^+ \rightarrow X\,^1\Sigma_g^+$ transition, obtained by excitation with the 785.843 nm output of the Ti:Sa laser, is shown in the upper part of Fig. 1. This series originates in an upper-state level with $J'=14$; $\{P(15),R(13)\}$ doublets are clearly observed for ground-state vibrational levels up to $v''=113$. Fainter lines around these *P-R* doublets correspond to transitions from neighboring collisionally populated rotational

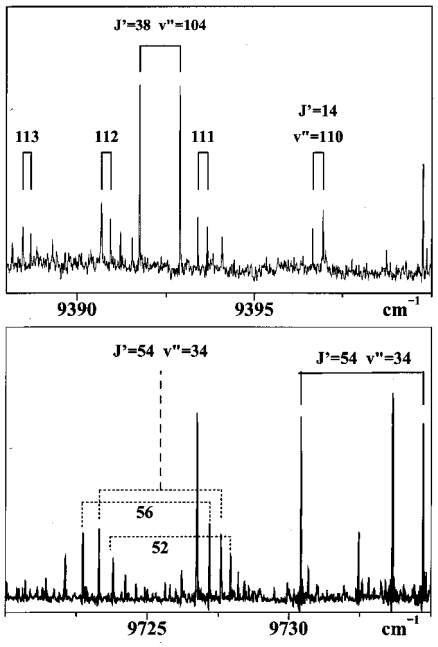

FIG. 1. Two examples of Ti:Sa laser-induced spectra. *Upper segment*: with the laser set at 785.843 nm, vibrational levels are observed up to $v''=113$ in a series with $J'=14$; *lower segment*: with the laser set at 869.440 nm, the doublet linked by solid lines are $P(55)$ and $R(53)$ transitions originating in an *A*-state level with $J'=54$. The $J'=54$ doublet joined with dashed lines corresponds to transitions from a collisionally populated $b\,^3\Pi_u$-state level down to the same $v''=34$ ground state level; the additional doublets labeled 56 and 52 arise from collisional rotational energy transfer in that triplet state.

levels. The lower portion of Fig. 1 shows a small portion of the fluorescence spectrum induced by the 869.440 nm laser line, which generates a $J'=54$ series of the $^{85,87}Rb_2$ isotopomer, together with an additional structure due to collisional transfer of an upper-state population. Such multiline patterns, also observed for NaLi and RbCs,[11,12] occur all along this $J'=54$ series, and are probably due to collisional transfer from the initially excited $A\,^1\Sigma_u^+$ level into levels of the nearby $b\,^3\Pi_u$ state.

The dataset generated in this way consists of 12 148 transitions in 424 fluorescence series. Use of the previously reported ground-state constants[1] made their assignment quite straightforward. Of the observed lines, 7009 belonged to the most abundant (52.1%) isotopomer $^{85,85}Rb_2$, 5044 to the mixed isotopomer $^{85,87}Rb_2$ (40.2% abundance), and 95 to $^{87,87}Rb_2$ (7.8% abundance). For each vibrational level, the range of associated rotational levels is indicated in Fig. 2. This dataset includes levels with rotational quantum numbers ranging from $J''=8$ to 243, which considerably extends the previously reported dataset and places severe demands on our analysis procedure. A complete listing of this dataset may be obtained from the Journal's electronic archive.[13]

III. ANALYSIS

In all of the fits reported herein, the observed transition energies were weighted by the inverse square of their estimated uncertainties of 0.001 cm^{-1}, and the quality of fit is characterized by the value of dimensionless standard error,[14]

$$\overline{\sigma}_f=\left[\frac{1}{N-M}\sum_{i=1}^{N}\left(\frac{y_{\rm calc}(i)-y_{\rm obs}(i)}{u(i)}\right)^2\right]^{1/2}, \quad (1)$$

where each of the N experimental data $y_{\rm obs}(i)$ has an uncertainty of $u(i)$, and $y_{\rm calc}(i)$ is the value of datum i predicted by the M-parameter model being fitted. All parameter uncertainties quoted herein are 95% confidence limit uncertainties, and the atomic masses used in the combined-isotopomer analysis were taken from the 1993 mass table.[15] In order to simplify the representation of these datasets, to extract the most physically meaningful molecular parameters and properties, and to allow a search for Born–Oppenheimer breakdown effects, all of the analyses reported below were based on combined-isotopomer fits in which all of the data for all three isotopomers were treated simultaneously.

The data used in the analyses reported below consisted only of the new *A-X* emission measurements described above. The PAS study of Ref. 3 did observe a dozen levels lying much closer to dissociation, but they are perturbed by triplet states sharing the same dissociation limit and split by hyperfine coupling interactions, and the coupled-channel calculations required for their analysis[3] are not readily combined with the more conventional single-channel data analysis techniques required to accurately describe the rest of the data for this state. As a result, the PAS measurements themselves were not used here, although the dissociation energy determined in Ref. 3 was utilized in the (recommended) ''direct-potential-fit'' analysis of Sec. III C.

A. Unconstrained combined-isotopomer Dunham-type analysis

The observed transitions for isotopomer α of species $A-B$ formed from atoms of mass M_A^α and M_B^α were expressed as differences between level energies, written as[16]

$$E^\alpha(v,J)=\sum_{(l,m)\neq(0,0)}Y_{l,m}^1\left(\frac{\mu_1}{\mu_\alpha}\right)^{m+l/2}(v+1/2)^l[J(J+1)]^m + \sum_{(l,m)\geqslant(0,0)}\left\{\frac{\Delta M_A^\alpha}{M_A^\alpha}\delta_{l,m}^A+\frac{\Delta M_B^\alpha}{M_B^\alpha}\delta_{l,m}^B\right\} \times\left(\frac{\mu_1}{\mu_\alpha}\right)^{m+l/2}(v+1/2)^l[J(J+1)]^m, \quad (2)$$

where $\Delta M_A^\alpha=M_A^\alpha-M_A^1$, and $\alpha=1$ identifies a selected reference species, in this case the most abundant isotopomer, $^{85,85}Rb_2$. This expression is equivalent to the familiar Ross–Eng–Kildal–Bunker–Watson[17–19] expansion, except that the Born–Oppenheimer and JWKB breakdown terms in the second sum are included as additive rather than multiplicative corrections, and the reference species (isotopomer $\alpha=1$, $^{85,85}Rb_2$) is a real physical molecule. The conventional Dunham constants for other ($\alpha\neq1$) isotopomers are therefore not independent, but may be generated from the expression

$$Y_{l,m}^\alpha=\left(Y_{l,m}^l+\frac{\Delta M_A^\alpha}{M_A^\alpha}\delta_{l,m}^A+\frac{\Delta M_B^\alpha}{M_B^\alpha}\delta_{l,m}^B\right)\left(\frac{\mu_1}{\mu_\alpha}\right)^{m+l/2}. \quad (3)$$

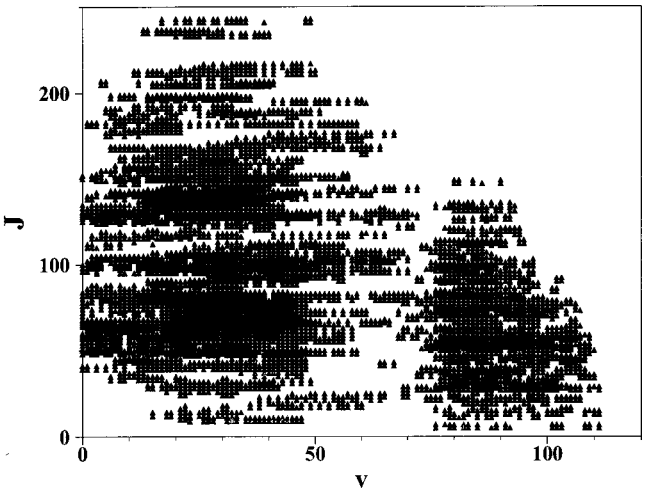

FIG. 2. The data field $\{v,J\}$ for the $X\,^1\Sigma_g^+$ ground state of Rb_2.

Other advantages of this expansion are discussed elsewhere.[16]

Our complete three-isotopomer dataset was fitted to Eq. (2) using program ''DSParFit,''[20] which simplifies the resulting parameters by applying the sequential rounding and refitting procedure described in Ref. 14. After experimentation to determine the optimum length $l_{\rm max}(m)$ for the vibrational expansion associated with each power (m) of $[J(J+1)]$, this yielded the molecular constants given in the first column of Table I. Within the experimental uncertainties, no Born–Oppenhiemer breakdown parameters were required to fit this multi-isotopomer dataset.

For the user's convenience, the Dunham parameters for the minority isotopomers, as generated by substituting the fitted parameters of column 1 into Eq. (3) and rounded at the first digit of the parameter sensitivity,[14] are shown in the last two columns of Table I. Relatively more significant digits are required to represent these derived constants adequately, as the compensating changes associated with the sequential rounding and refitting procedure do not come into play. The results in the last row of this table show that these derived constants reproduce the data for the individual minority isotopomers with no significant loss of precision. In particular, the value of $\overline{\sigma}_f$ under the $^{85,85}Rb_2$ column is that for the full combined-isotopomer fit to 62 Dunham parameters and 424 fluorescence origins, while the values for $^{85,87}Rb_2$ and $^{87,87}Rb_2$ are associated with fits in which the Dunham parameters were fixed at the values derived from the global analysis and only the fluorescence origin energies for that isotopomer were free parameters.

B. Constrained-CDC combined-isotopomer Dunham-type analysis

It has long been known that centrifugal distortion constants (CDCs) of diatomic molecules,

$$K_m(v)=\sum_{l=0}^{l_{\rm max}(m)}Y_{l,m}(v+1/2)^l[J(J+1)]^m, \quad (4)$$

for $m\geqslant2$ [$K_2(v)=-D_v$, $K_3(v)=H_v$,..., etc.], are not independent physical parameters, but are determined by and

TABLE I. Parameters for the $X\ ^1\Sigma_g^+$ state of Rb_2 obtained from a simultaneous fit of 12 148 visible transition frequencies to the energy level differences as defined by Eq. (2); the numbers in parentheses are 95% confidence limit uncertainties.

	From all-isotopomer fit		From the $^{85}Rb^{85}Rb$ constants and Eq. (3)	
	$^{85}Rb^{85}Rb$		$^{85}Rb^{87}Rb$	$^{87}Rb^{87}Rb$
$Y_{1,0}$	57.789 159 4	$(\pm 1.2\times10^{-3})$	57.456 164 659	57.121 228 72
$Y_{2,0}$	−0.139 558 03	$(\pm 4.8\times10^{-4})$	−0.137 954 331 35	−0.136 350 632 7
$Y_{3,0}$	$-3.967\,991\times10^{-4}$	$(\pm 1.1\times10^{-4})$	$-3.899\,791\,998\times10^{-4}$	$-3.831\,988\,254\times10^{-4}$
$Y_{4,0}$	$3.432\,253\times10^{-5}$	$(\pm 1.6\times10^{-5})$	$3.353\,824\,351\,8\times10^{-5}$	$3.276\,302\,156\,4\times10^{-5}$
$Y_{5,0}$	$-3.791\,364\,6\times10^{-6}$	$(\pm 1.5\times10^{-6})$	$-3.683\,382\,550\,49\times10^{-6}$	$-3.577\,267\,102\,94\times10^{-6}$
$Y_{6,0}$	$2.692\,152\,3\times10^{-7}$	$(\pm 9.7\times10^{-8})$	$2.600\,405\,978\,31\times10^{-7}$	$2.510\,768\,125\,78\times10^{-7}$
$Y_{7,0}$	$-1.361\,418\,8\times10^{-8}$	$(\pm 4.5\times10^{-9})$	$-1.307\,445\,303\,54\times10^{-8}$	$-1.255\,017\,809\,25\times10^{-8}$
$Y_{8,0}$	$5.026\,788\,2\times10^{-10}$	$(\pm 1.5\times10^{-10})$	$4.799\,683\,806\,84\times10^{-10}$	$4.580\,362\,977\,7\times10^{-10}$
$Y_{9,0}$	$-1.378\,327\,7\times10^{-11}$	$(\pm 3.8\times10^{-12})$	$-1.308\,473\,044\,44\times10^{-11}$	$-1.241\,403\,474\,33\times10^{-11}$
$Y_{10,0}$	$2.832\,098\,9\times10^{-13}$	$(\pm 7.2\times10^{-14})$	$2.673\,073\,906\,58\times10^{-13}$	$2.521\,274\,034\,63\times10^{-13}$
$Y_{11,0}$	$-4.369\,351\times10^{-15}$	$(\pm 1.0\times10^{-15})$	$-4.100\,244\,363\,9\times10^{-15}$	$-3.844\,852\,941\,61\times10^{-15}$
$Y_{12,0}$	$5.032\,431\times10^{-17}$	$(\pm 1.1\times10^{-17})$	$4.695\,273\,450\,13\times10^{-17}$	$4.377\,153\,652\,82\times10^{-17}$
$Y_{13,0}$	$-4.260\,08\times10^{-19}$	$(\pm 8.7\times10^{-20})$	$-3.951\,764\,644\,31\times10^{-19}$	$-3.662\,544\,258\,97\times10^{-19}$
$Y_{14,0}$	$2.571\,91\times10^{-21}$	$(\pm 4.9\times10^{-22})$	$2.372\,025\,419\,33\times10^{-21}$	$2.185\,606\,921\,54\times10^{-21}$
$Y_{15,0}$	-1.0477×10^{-23}	$(\pm 1.9\times10^{-24})$	$-9.607\,065\,921\,06\times10^{-24}$	$-8.800\,440\,232\,54\times10^{-24}$
$Y_{16,0}$	2.58×10^{-26}	$(\pm 4.3\times10^{-27})$	$2.352\,143\,360\,08\times10^{-26}$	$2.142\,093\,007\,12\times10^{-26}$
$Y_{17,0}$	-2.9×10^{-29}	$(\pm 4.5\times10^{-30})$	$-2.628\,647\,400\,5\times10^{-29}$	$-2.379\,949\,703\,28\times10^{-29}$
$Y_{0,1}$	$2.240\,433\,6\times10^{-2}$	$(\pm 6.1\times10^{-7})$	$2.214\,688\,178\times10^{-2}$	$2.188\,942\,756\times10^{-2}$
$Y_{1,1}$	$-5.581\,67\times10^{-5}$	$(\pm 2.4\times10^{-7})$	$-5.485\,736\,23\times10^{-5}$	$-5.390\,358\,47\times10^{-5}$
$Y_{2,1}$	$-3.355\,13\times10^{-7}$	$(\pm 5.3\times10^{-8})$	$-3.278\,463\,65\times10^{-7}$	$-3.202\,683\,38\times10^{-7}$
$Y_{3,1}$	$1.372\,64\times10^{-8}$	$(\pm 6.3\times10^{-9})$	$1.333\,545\,77\times10^{-8}$	$1.295\,127\,331\times10^{-8}$
$Y_{4,1}$	$-1.702\,632\times10^{-9}$	$(\pm 4.5\times10^{-10})$	$-1.644\,607\,711\times10^{-9}$	$-1.587\,916\,908\times10^{-9}$
$Y_{5,1}$	$9.857\,78\times10^{-11}$	$(\pm 2.1\times10^{-11})$	$9.466\,967\,963\times10^{-11}$	$9.087\,350\,241\times10^{-11}$
$Y_{6,1}$	$-3.520\,313\times10^{-12}$	$(\pm 6.5\times10^{-13})$	$-3.361\,269\,388\,9\times10^{-12}$	$-3.207\,676\,690\,1\times10^{-12}$
$Y_{7,1}$	$8.074\,27\times10^{-14}$	$(\pm 1.4\times10^{-14})$	$7.665\,060\,093\,1\times10^{-14}$	$7.272\,165\,27\times10^{-14}$
$Y_{8,1}$	$-1.209\,93\times10^{-15}$	$(\pm 1.9\times10^{-16})$	$-1.141\,991\,302\,56\times10^{-15}$	$-1.077\,139\,323\,32\times10^{-15}$
$Y_{9,1}$	$1.17\,177\times10^{-17}$	$(\pm 1.8\times10^{-18})$	$1.099\,601\,139\,46\times10^{-17}$	$1.031\,110\,416\,94\times10^{-17}$
$Y_{10,1}$	-7.023×10^{-20}	$(\pm 1.1\times10^{-20})$	$-6.552\,480\,389\,8\times10^{-20}$	$-6.108\,528\,880\,7\times10^{-20}$
$Y_{11,1}$	2.347×10^{-22}	$(\pm 3.8\times10^{-23})$	$2.177\,140\,246\,2\times10^{-22}$	$2.017\,800\,458\,2\times10^{-22}$
$Y_{12,1}$	-3.3×10^{-25}	$(\pm 5.8\times10^{-26})$	$-3.043\,529\,472\times10^{-25}$	$-2.804\,337\,182\times10^{-25}$
$Y_{0,2}$	$-1.356\,72\times10^{-8}$	$(\pm 5.6\times10^{-11})$	$-1.325\,718\,29\times10^{-8}$	$-1.295\,074\,89\times10^{-8}$
$Y_{1,2}$	-5.711×10^{-11}	$(\pm 1.9\times10^{-11})$	$-5.548\,345\times10^{-11}$	$-5.388\,501\times10^{-11}$
$Y_{2,2}$	-1.5734×10^{-12}	$(\pm 3.4\times10^{-12})$	$-1.519\,779\,8\times10^{-12}$	$-1.467\,391\,9\times10^{-12}$
$Y_{3,2}$	-4.7516×10^{-13}	$(\pm 3.3\times10^{-13})$	$4.563\,222\,65\times10^{-13}$	$-4.380\,241\,13\times10^{-13}$
$Y_{4,2}$	$7.196\,87\times10^{-14}$	$(\pm 2.0\times10^{-14})$	$6.871\,723\,857\times10^{-14}$	$6.557\,721\,47\times10^{-14}$
$Y_{5,2}$	$-4.613\,12\times10^{-15}$	$(\pm 7.9\times10^{-16})$	$-4.379\,323\,706\times10^{-15}$	$-4.154\,848\,803\,7\times10^{-15}$
$Y_{6,2}$	$1.660\,68\times10^{-16}$	$(\pm 2.1\times10^{-17})$	$1.567\,431\,269\,9\times10^{-16}$	$1.478\,419\,190\,7\times10^{-16}$
$Y_{7,2}$	$-3.654\,61\times10^{-18}$	$(\pm 3.8\times10^{-19})$	$-3.429\,523\,985\,3\times10^{-18}$	$-3.215\,909\,641\,7\times10^{-18}$
$Y_{8,2}$	5.0119×10^{-20}	$(\pm 4.5\times10^{-21})$	$4.676\,117\,964\,6\times10^{-20}$	$4.359\,296\,012\,7\times10^{-20}$
$Y_{9,2}$	-4.1762×10^{-22}	$(\pm 3.3\times10^{-23})$	$-3.873\,955\,303\,1\times10^{-22}$	$-3.590\,429\,600\,9\times10^{-22}$
$Y_{10,2}$	1.933×10^{-24}	$(\pm 1.4\times10^{-25})$	$1.782\,770\,445\,1\times10^{-24}$	$1.642\,661\,749\,2\times10^{-24}$
$Y_{11,2}$	-3.81×10^{-27}	$(\pm 2.5\times10^{-28})$	$-3.493\,645\,238\times10^{-27}$	$-3.200\,312\,808\times10^{-27}$
$Y_{0,3}$	1.129×10^{-14}	$(\pm 2.2\times10^{-15})$	$1.090\,524\,6\times10^{-14}$	$1.052\,933\,5\times10^{-14}$
$Y_{1,3}$	-1.7728×10^{-15}	$(\pm 6.7\times10^{-16})$	$-1.702\,517\,3\times10^{-15}$	$-1.634\,247\,7\times10^{-15}$
$Y_{2,3}$	3.0291×10^{-16}	$(\pm 9.6\times10^{-17})$	$2.892\,248\,82\times10^{-16}$	$2.760\,087\,94\times10^{-16}$
$Y_{3,3}$	-2.0947×10^{-17}	$(\pm 7.4\times10^{-18})$	$-1.988\,539\,07\times10^{-17}$	$-1.886\,610\,75\times10^{-17}$
$Y_{4,3}$	5.3849×10^{-19}	$(\pm 3.5\times10^{-19})$	$5.082\,532\,85\times10^{-19}$	$4.793\,903\,4\times10^{-19}$
$Y_{5,3}$	7.162×10^{-21}	$(\pm 1.0\times10^{-20})$	$6.720\,895\,19\times10^{-21}$	$6.302\,271\,61\times10^{-21}$
$Y_{6,3}$	-8.042×10^{-22}	$(\pm 2.2\times10^{-22})$	$-7.503\,210\,493\times10^{-22}$	$-6.994\,843\,978\times10^{-22}$
$Y_{7,3}$	2.1403×10^{-23}	$(\pm 3.1\times10^{-24})$	$1.985\,399\,773\,8\times10^{-23}$	$1.840\,093\,021\,1\times10^{-23}$
$Y_{8,3}$	-2.811×10^{-25}	$(\pm 2.9\times10^{-26})$	$-2.592\,533\,741\times10^{-25}$	$-2.388\,785\,399\,4\times10^{-25}$
$Y_{9,3}$	1.867×10^{-27}	$(\pm 1.6\times10^{-28})$	$1.711\,977\,863\times10^{-27}$	$1.568\,237\,273\times10^{-27}$
$Y_{10,3}$	$-5.\times10^{-30}$	$(\pm 3.7\times10^{-31})$	$-4.558\,417\,36\times10^{-30}$	$-4.151\,343\,04\times10^{-30}$
$Y_{0,4}$	-5.37×10^{-20}	$(\pm 3.0\times10^{-20})$	$-5.127\,39\times10^{-20}$	$-4.893\,09\times10^{-20}$
$Y_{1,4}$	2.348×10^{-20}	$(\pm 9.2\times10^{-21})$	$2.229\,001\,6\times10^{-20}$	$2.114\,747\,7\times10^{-20}$
$Y_{2,4}$	-4.472×10^{-21}	$(\pm 1.2\times10^{-21})$	$-4.220\,893\times10^{-21}$	$-3.981\,194\,8\times10^{-21}$
$Y_{3,4}$	3.847×10^{-22}	$(\pm 8.4\times10^{-23})$	$3.610\,064\,76\times10^{-22}$	$3.385\,205\,09\times10^{-22}$
$Y_{4,4}$	-1.7873×10^{-23}	$(\pm 3.4\times10^{-24})$	$-1.667\,556\,344\times10^{-23}$	$-1.554\,574\,066\times10^{-23}$
$Y_{5,4}$	4.765×10^{-25}	$(\pm 8.0\times10^{-26})$	$4.420\,142\times10^{-25}$	$4.096\,642\,17\times10^{-25}$
$Y_{6,4}$	-7.29×10^{-27}	$(\pm 1.1\times10^{-27})$	$-6.723\,433\,29\times10^{-27}$	$-6.195\,035\,77\times10^{-27}$
$Y_{7,4}$	5.94×10^{-29}	$(\pm 8.4\times10^{-30})$	$5.446\,785\,49\times10^{-29}$	$4.989\,464\,06\times10^{-29}$
$Y_{8,4}$	$2.\times10^{-31}$	$(\pm 2.6\times10^{-32})$	$1.823\,366\,95\times10^{-31}$	$-1.660\,537\,21\times10^{-31}$
No. of data	12 148		5044	95
No. parameters	486		171	7
$\overline{\sigma_f}$	1.031		1.070	0.998

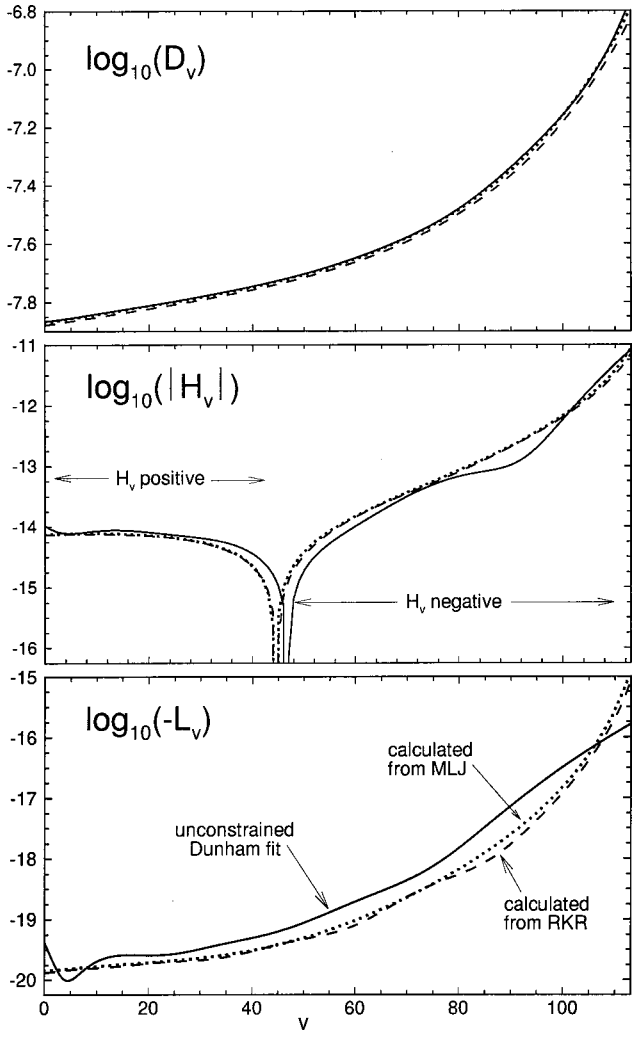

FIG. 3. A comparison of empirical CDCs from unconstrained fit (solid curves) with values calculated from the initial RKR potential (dashed curves) and from the final recommended analytic MLJ potential of Table II.

can be calculated from a knowledge of the potential energy function.[21–25] They are therefore implicitly determined by a knowledge of the vibrational energies $[G_v = K_0(v)]$ and inertial rotational constants $[B_v = K_1(v)]$ whose use in the RKR inversion procedure[26] yields the potential function. As a result, while unconstrained Dunham-type analyses such as that described above can usually provide accurate empirical representations of experimental datasets, the resulting CDCs tend to be ''effective'' parameters incorporating effects due to perturbations, interparameter correlation, and the neglect of undetermined higher-order CDCs. This means that the resulting term-value expressions will not be reliable for extrapolation to higher J values, and that small compensating errors are introduced into the fitted G_v and B_v values, and hence into the potential function determined from them. As an illustration of this problem for the present system, Fig. 3 compares CDCs for $^{85,85}Rb_2$ generated from the unconstrained-fit empirical parameters listed in Table I (solid curves) with values calculated numerically[27] from the RKR potential generated[28] from the G_v and B_v expansions presented there (dashed curves), and also with CDCs calculated from the final recommended ''MLJ'' potential of Sec. III C. The error in the unconstrained-fit CDCs clearly increases with order (from D_v to H_v to L_v); for L_v $(m=4)$ it is typically much greater than a factor of 2, and for orders $m \geqslant 5$ empirical CDCs could not even be determined.

A widely used approach for addressing this problem involves calculating CDCs from an initial RKR potential computed from G_v and B_v expressions obtained from an initial unconstrained fit. These CDCs are then held fixed in a new fit to the original dataset to obtain improved G_v and B_v expansions, which, in turn, are used to generate an improved RKR potential and then improved CDCs. In a wide variety of applications this iterative self-consistent procedure has been found to converge after very few cycles.[1,25,29–31] However, when applied to Rb_2 $X\,^1\Sigma_g^+$ in Ref. 1, it was found wanting, since the computational tools then available[9] could only calculate the first four CDCs (D_v, H_v, L_v, and M_v), and this was inadequate to describe the existing dataset. Neglect of several hundred high-J data circumvented this problem and allowed a fairly reliable potential energy curve to be obtained, but the resulting molecular band constants $\{G_v, B_v, D_v, \ldots, M_v\}$ could not accurately describe all of the existing data, and certainly would not yield accurate predictions for even higher J values.

Since that time a generally accessible computer code able to calculate the first six CDCs [up to $K_7(v) = O_v$] has become available.[27] However, even the inclusion of the two additional calculated CDCs does not explain all of our accurate high-J data for this system. In particular, with the first six CDCs fixed at values calculated[27] from the RKR potential generated[28] from the G_v and B_v expansions ($\{Y_{l,m}\}$ for $m=0$ and 1) in Table I, a fit to the full (12 148 data) three-isotopomer dataset gave a dimensionless standard error of $\overline{\sigma}_f = 5.9$, and iterating to self-consistency only reduced this value to 3.0. Reducing the range of rotational levels considered from the dataset maximum of $J=243$ to $J_{\max}=150$ (excluding 1584 data) reduces $\overline{\sigma}_f$ to 1.26, and truncating the range further by setting $J_{\max}=100$ (excluding an additional 3021 data) reduced $\overline{\sigma}_f$ to 1.07, which is the level of agreement attained in the full unconstrained-parameter analysis. This indicates that the problem in the fit to the complete dataset was due to the lack of even higher-order CDC's $[K_m(v)$ for $m>7]$.[32] While the RKR potential obtained from the $J_{\max}=100$ reduced dataset would have been fairly reliable (see Sec. IV), the associated molecular parameters would be unable to represent a substantial fraction of the available data, and would be unreliable for extrapolation to higher J. The computation of yet higher-order CDC's is certainly possible (see, e.g., Ref. 33), but the numerical procedure tends to become increasingly unstable for the higher orders, and it is not even clear that the expansion in $[J(J+1)]$ truly converges. Thus, it seems clear that the data analysis approach of constraining the CDCs at their ''mechanically consistent'' calculated values and iterating the parameter-fit analysis to convergence is not adequate for the present system.

C. Combined-isotopomer direct-potential-fit (DPF) analysis

A more compact and more physically significant alternative to the traditional parameter-fit approach to data analysis is to fit the data directly to eigenvalue differences numerically calculated from the Schrödinger equation for some parametrized analytical potential energy function.[34–36] For diatomic molecules, most early applications of this approach (called the ''IPA'' method) involved fitting to determine analytic corrections to a pointwise RKR potential,[35–37] and that was the method used in the Rb_2 study of Ref. 1. More recently, the preferred approach has been to use direct fits to determine parameters characterizing fully analytic potential energy functions, and (where possible) to determine simultaneously atomic-mass-dependent radial and centrifugal potential corrections due to the breakdown of the Born–Oppenheimer approximation.[38–44]

Since Rb_2 has a relatively large reduced mass, Born–Oppenheimer breakdown effects are expected to be small. Both the parameter-fit analyses described above and exploratory direct-potential-fit (DPF) analyses showed that within the precision of the available data for Rb_2 ($X\,^1\Sigma_g^+$), their effect is negligible. As a result, the observed pattern of level energies for all three isotopomers can be described by the eigenvalues of the simple radial Schrödinger equation,

$$\left(-\frac{\hbar^2}{2\mu_\alpha}\frac{d^2}{dR^2}+V(R)+\frac{\hbar^2 J(J+1)}{2\mu_\alpha R^2}-E^\alpha_{v,J}\right)\psi_{v,J}(R)=0, \tag{5}$$

where $V(R)$ is the parametrized analytic potential function we wish to determine, μ_α is the reduced mass of the atoms forming isotopomer α, and $\{E^\alpha_{v,J}\}$ are its eigenvalues.

In the present work the potential energy was represented by the ''Modified Lennard-Jones'' (MLJ) function,[45]

$$V(R)=\mathcal{D}_e[1-(R_e/R)^n e^{-\beta(z)z}]^2, \tag{6}$$

where $\mathcal{D}_e$ is the well depth, R_e the equilibrium internuclear distance, $z\equiv(R-R_e)/(R+R_e)$, and $\beta(z)$ is a simple power series in z,

$$\beta(z)=\sum_{j=0}\beta_j z^j, \tag{7}$$

whose expansion parameters $\{\beta_j\}$ are dimensionless. Since the ground $X\,^1\Sigma_g^+$ state of Rb_2 dissociates to yield two ^1S state atoms, the asymptotic behavior of its potential energy curve is $V(R)\sim\mathcal{D}-C_6/R^6$, so the power n in our model MLJ potential for this state is $n=6$.[46–48] Our numerical treatment of Eq. (5) was performed on the interval $2.6\geqslant R\geqslant 42.0$ Å with a radial mesh of 0.001 Å. This is sufficient to ensure that all of the eigenvalues used in the fits were converged to better than 0.0002 cm^{-1}.

Optimization of the parameters of our model potential energy function started from an initial trial potential in which $\mathcal{D}_e$ was taken from Ref. 3, and R_e and the first three exponent parameters (β_0, β_1, and β_2) were calculated from the low-order molecular constants ($Y_{1,1}$, $Y_{1,0}$, and $Y_{2,0}$; see Table I) using Taylor series expansions matched to the Dunham relations.[49] In most of our fits $\mathcal{D}_e$ was held fixed at the value determined in Ref. 3, because it was based on data for levels lying much closer to dissociation than those included in the present analysis. Initial trial values of the higher-order exponent parameters β_j were estimated by a ''bootstrapping'' method that started by obtaining a good fit to a reduced dataset spanning a modest range of v, with all β_j values for $j\geqslant 3$ set to zero. In stages, the range of data included in the fit was then expanded and one additional β_j parameter (at a time) set free. Our practice was to initially free only this one additional parameter, and to then release the lower-order coefficients one by one in an attempt to minimize the occurrence of large changes that might destabilize the fit; however, other strategies may work equally well.

As the highest vibrational levels included in our dataset are bound by only a few wave numbers, it was initially hoped that the value of $\mathcal{D}_e$ could be treated as a free parameter and the fit used to determine an improved independent estimate of the ground-state dissociation energy. However, the values obtained from fits in which $\mathcal{D}_e$ was also set free differed from one another and from the current best estimate[3] of 3993.53 ($\pm$0.06) cm^{-1} by a number of wave numbers. The magnitude of these discrepancies was somewhat disconcerting. Further inspection showed that the associated $\beta(z)$ functions tended to grow very quickly beyond the range of the data, causing the potential to approach an asymptote relatively abruptly, which led to an underestimation of the dissociation energy. This rapid growth in $\beta(z)$ beyond the range of R spanned by the data is shown by the dashed curves (labeled ''unconstrained'') in Fig. 4. One implication of this behavior is that although the resulting MLJ potential will be ''well behaved,'' smoothly approaching its asymptote with the theoretically predicted $\mathcal{D}-C_6/R^6$ behavior, the value of the C_6 coefficient, defined within the MLJ form by the expression

$$C_6=2\mathcal{D}_e(R_e)^6 e^{-\beta_\infty}, \tag{8}$$

where $\beta_\infty\equiv\beta(z=1)=\beta[z(R=\infty)]$, is unconstrained, and while finite, it is (in this case) unrealistically large.

Our initial attempt to address this problem involved defining the highest-order coefficient ($\beta_j=\beta_{\rm last}$) in the power series expansion for $\beta(z)$ in terms of both the other coefficients and a fixed limiting value of

$$\beta_\infty=\ln[2\mathcal{D}_e(R_e)^6/C_6], \tag{9}$$

determined by the theoretically known[50] C_6 constant for this species:

$$\beta_{\rm last}=\beta_\infty-\sum_{j=0}^{\rm last-1}\beta_j=\ln[2\mathcal{D}_e(R_e)^6/C_6]-\sum_{j=0}^{\rm last-1}\beta_j. \tag{10}$$

This constraint did successfully force $\beta(z)$ to reach the theoretical limit of $\beta_\infty\approx 0.676$. However, as sometimes found by Hajigeorgiou and Le Roy,[45] beyond the region governed by the data, the resulting $\beta(z)$ function had an implausibly large maximum, following the ''unconstrained'' curves off scale in Fig. 4, and only dropping back toward the 0.676 limit at very large R, and the fit still underestimated the dissociation energy by a number of wave numbers.

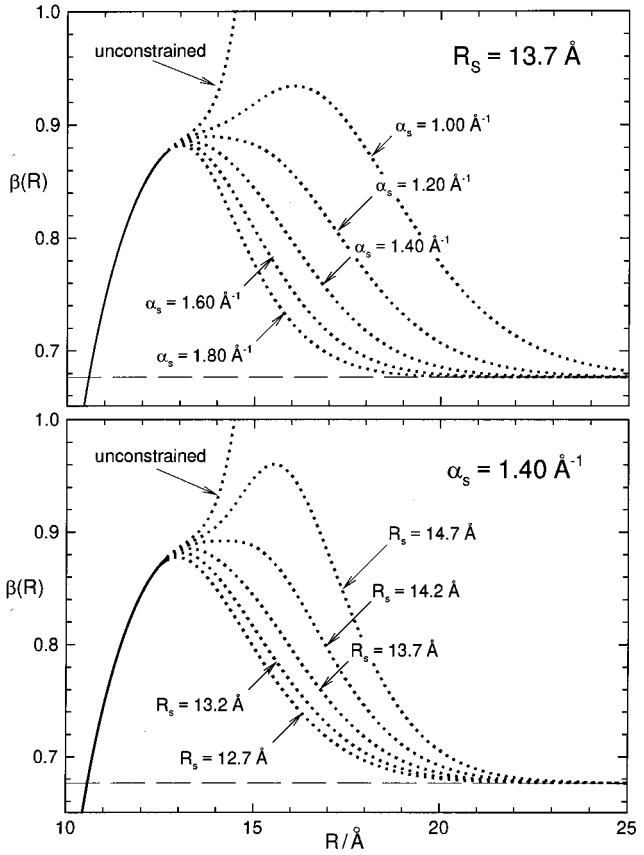

FIG. 4. Fitted $\beta_S(R)$ function determined for various $\{\alpha_s, R_s\}$ combinations.

TABLE II. Parameters defining the switched MLJ potential of Eqs. (6), (11), and (12) for the $X\,^1\Sigma_g^+$ state of Rb_2, determined from a direct fit to our data for all three isotopomers. The numbers in parentheses are 95% confidence limit uncertainties, and the 424 fitting parameters not listed are the origins of the 424 fluorescence series.

$\mathcal{D}_e$ /cm^{-1}	3993.53[a]	(±0.06)[a]
R_e /Å^{-1}	4.209 951 49	($\pm 7.0\times10^{-6}$)
β_0 /Å^{-1}	−5.890 539 6	($\pm 1.4\times10^{-5}$)
β_1 /Å^{-1}	$1.212\,348\,8\times10^{1}$	($\pm 8.8\times10^{-4}$)
β_2 /Å^{-1}	$1.437\,536\times10^{1}$	($\pm 3.0\times10^{-3}$)
β_3 /Å^{-1}	$3.236\,17\times10^{1}$	($\pm 1.6\times10^{-1}$)
β_4 /Å^{-1}	7.3117×10^{1}	($\pm 4.9\times10^{-1}$)
β_5 /Å^{-1}	-4.0307×10^{2}	($\pm 1.4\times10^{1}$)
β_6 /Å^{-1}	$1.659\,16\times10^{3}$	($\pm 7.2\times10^{1}$)
β_7 /Å^{-1}	-9.6104×10^{3}	($\pm 4.7\times10^{2}$)
β_8 /Å^{-1}	-7.3975×10^{4}	($\pm 4.3\times10^{3}$)
β_9 /Å^{-1}	4.502×10^{5}	($\pm 6.3\times10^{3}$)
β_{10} /Å^{-1}	3.19×10^{5}	($\pm 7.2\times10^{4}$)
β_{11} /Å^{-1}	-7.046×10^{6}	($\pm 3.6\times10^{5}$)
β_{12} /Å^{-1}	1.9519×10^{7}	($\pm 8.0\times10^{5}$)
β_{13} /Å^{-1}	-2.298×10^{7}	($\pm 8.7\times10^{5}$)
β_{14} /Å^{-1}	1.03×10^{7}	($\pm 3.9\times10^{5}$)
C_6 /cm^{-1} Å (Ref. 6)	2.261×10^{7}	($\pm 1.1\times10^{5}$)[b]
α_s /Å^{-1}	1.4	
R_s /Å	13.7	
No. of data	12 148	
No. parameters	440	
$\overline{\sigma_f}$	1.157	

[a]Value and uncertainty from Ref. 3.
[b]Value and uncertainty from Ref. 50.

Our final solution was simply to follow the approach of Ref. 45 and introduce a switching function parametrized to make $\beta(z)$ beyond the range of the experimental data smoothly approach the asymptotic limit defined by the theoretical C_6 value. This switching function has the form[45]

$$\beta_S(z) = f_S(R)\left(\sum_{j=0}^{\text{last}} \beta_j z^j - \beta_\infty\right) + \beta_\infty, \tag{11}$$

$$f_S(R) = 1/[e^{\alpha_S(R-R_S)}+1], \tag{12}$$

where the parameters α_S and R_S are chosen to ensure that $\beta(z)$ ''looks'' smooth.

To determine optimum switching-function parameters, we performed global fits to the data for a range of ''plausible'' trial sets of $\{\alpha_S, R_S\}$ values. In all cases the quality of fit to the data was essentially the same, and the criterion applied was a desire to obtain a $\beta_S(R)$ function that would approach the theoretically known limiting value ($\beta_\infty \approx 0.676$) in the most ''reasonable'' manner. Since R_S is the distance at which the switching function turns on, it seems reasonable to make it larger than the outer turning point for the highest observed vibrational level (here $v=113$, with outer turning point *ca.* 12.7 Å) so that the switching function would not interfere significantly with the behavior of $\beta_S(R)$ in the region governed by the data. Because the strength or abruptness of the switching function increases with the value of α_S, it was chosen to have the smallest value which would force $\beta_S(z)$ to the proper long range limit without showing either implausible extrema or an abrupt change in the shape of $\beta_S(z)$ beyond the range of the data. The several curves in the two segments of Fig. 4 show the $\beta_S(R)$ functions associated with a number of these trial fits.

While there is no unique optimum choice of switching function, we chose to determine our final recommended potential using $\alpha_S = 1.40\,\text{Å}^{-1}$ and $R_S = 13.7\,\text{Å}$. The resulting potential expansion parameters are listed in Table II; again, these parameters are rounded without loss of precision using the sequential rounding and refitting procedure of Ref. 14. This final recommended potential is defined by Eqs. (6), (11), and (12), with the value of β_∞ appearing in Eq. (11) being defined by Eq. (9) using the values of $\mathcal{D}_e$, R_e, and[50] C_6 precisely as listed in Table II.

An alternate approach to the determination of the MLJ potential switching function parameters might be to treat them as variables to be determined via the least-squares fit to the experimental data (see, e.g., Ref. 51). However, such an approach offers no way of readily imposing the essential requirement that beyond the range of the data $\beta_S(R)$ should approach the limiting value (β_∞) determined by the known C_6 long-range potential coefficient in the most ''reasonable'' manner possible. Moreover, since the objective in introducing the switching function is to moderate the behavior of $\beta_S(R)$ *beyond* the range of the experimental data, it would seem contradictory to use the fit to define that function. Thus the case-by-case manual determination of optimum α_S and R_S values seems to be an unavoidable feature of use of the MLJ potential.

D. Fitting to determine the dissociation energy

A slightly disappointing feature of the DPF analysis described above is the fact that the fits seem unable to determine a reliable value for the dissociation energy $\mathcal{D}_e$. This seems to be a general problem associated with most analytic model potentials in direct fits to data for many-level systems.[40,41,44,51] For ground-state Rb_2 the independent coupled-channel analysis of the PAS data for levels lying extremely close to dissociation yielded a reliable $\mathcal{D}_e$ that was held fixed in our analysis,[3] but that is a special situation that does not usually arise. Moreover, unconstrained- or constrained-CDC Dunham-expansion fits such as those described in Secs. III A and III B are of no help, since such empirical polynomials in $(v+1/2)$ are generally unreliable for vibrational extrapolation. For example, although the highest vibrational level used in our analysis ($v=113$) is only bound by 7 cm^{-1}, a vibrational extrapolation using the Dunham parameters of Table I predicts $v_{\mathcal{D}} \approx 118.1$, and hence misses almost half of the $(9-10)$ levels lying above $v=113$.[3]

The ideal solution to this problem would be the development and application of a better analytic model potential energy function that is more robust and stable in the extrapolation region. In the meantime, however, we note that an alternate type of parameter-fit analysis can provide reliable values of $\mathcal{D}_e$ that can then be held fixed in the global direct potential fit to the data.

It has long been known that particularly reliable vibrational energy extrapolations may be obtained from fits of observed level energies to ''near-dissociation expansion'' (NDE) expressions that incorporate the theoretically known[52,53] limiting near-dissociation behavior of vibrational level spacings.[54,55] We therefore fitted the vibrational energies of the 20 highest levels in the present dataset ($v=94-113$) to such expansions,[56] while fixing the values of the two longest-range inverse-power potential coefficients (C_6 and C_8) at their known theoretical values.[50,57] This approach predicts $\mathcal{D}_e = 3993.47(\pm 0.18)$ cm^{-1} and $v_{\mathcal{D}} = 123.01(\pm 0.19)$, values remarkably close to the PAS results[3] $\mathcal{D}_e = 3993.53(\pm 0.06)$ cm^{-1} and $v_{\mathcal{D}} = 122.994(\pm 0.012)$, respectively. The PAS results should be more reliable, since the binding energies of the highest levels used in that analysis are orders of magnitude smaller than those for the levels used in our NDE fits. However, the results obtained from the latter are clearly very good, and provide confidence that fits to NDE functions should be able to provide the reliable dissociation energies that the DPF method is not (yet) able to provide independently.

IV. DISCUSSION AND CONCLUSIONS

In the present paper we present new high-resolution resolved fluorescence data characterizing the ground electronic state of Rb_2 over essentially the whole potential energy well. These data are analyzed using three distinctly different approaches. Of these, the unconstrained Dunham fit and DPF analyses are of equivalent quality, both representing all of the available data within their uncertainties (of *ca.* ± 0.001 cm^{-1}), while the ''mechanically consistent'' constrained-CDC Dunham-type fits cannot properly account for the high-J data. Of the two successful fitting schemes, the DPF analysis is preferred for a number of reasons. In particular, we have the following.

(i) The 16 fitted potential parameters of the DPF analysis provide a much more compact representation of the 12 148 experimental data than do the 62 independent Dunham parameters of Table I. It might be argued that the DPF results are less convenient to use for predicting unobserved levels or transitions. However, because of the numbers of coefficients and significant digits involved, the Dunham parameters of Table I would only practically be utilized through their substitution into some computer program. If one is to use a computer program, the MLJ potential parameters of Table II may be equally readily input into one of the available easy-to-use Schrödinger-solver programs that can readily generate arbitrary numbers of eigenvalues or eigenvalue differences (together with any desired expectation values or matrix elements) for any specified analytic potential energy function (see, e.g., Ref. 27).

(ii) The resulting DPF-determined potential energy function is quantum mechanically accurate, while a potential function determined by the RKR method from the Dunham constants of Table I would only be as accurate as the first-order JWKB approximation on which the RKR inversion procedure is based. Moreover, the RKR-based approach cannot take full account of Born–Oppenheimer breakdown corrections. While these are not serious drawbacks for Rb_2 (see below), they could introduce substantial errors in treatments of small-reduced-mass species.

(iii) The recommended MLJ potential should yield reliable predictions for arbitrarily large J, while long J extrapolations with unconstrained molecular constants such as those of Table I are quite unreliable.

(iv) The recommended MLJ potential should yield realistic predictions for most vibrational levels above the highest one used in our analysis, while vibrational extrapolations with unconstrained high-order Dunham polynomials often behave very badly (see, e.g., Fig. 4 of Ref. 31). In the present case vibrational extrapolation with the Dunham parameters of Table I suggests that only five vibrational levels lie above the highest level used in our analysis ($v=113$), while our MLJ potential supports all of the nine additional levels predicted by the PAS analysis of Ref. 3, and agrees (within the uncertainties) with their prediction for the effective vibrational index at dissociation $v_{\mathcal{D}}$.

The constrained-CDC Dunham-type analysis of Sec. III B is certainly unsatisfactory, in that it could not quantitatively account for the experimental data at high J. On the other hand, it seems appropriate to ask whether that type of approach could yield a reliable potential energy curve if the analysis simply neglected any high-J data that cannot be accounted for by the limited number (six) of CDCs one can readily calculate. As a test of this question we applied the iterative self-consistent procedure of Sec. III B to our new dataset for Rb_2, while omitting the 4605 transitions associated with $J'' > 100$.[32] In the plots of Fig. 3, the CDCs calculated from the RKR curve generated from this analysis would be essentially identical to those calculated from our

final recommended MLJ potential function. However, a fit of our full 3-isotopomer 12 148-line dataset to eigenvalues calculated from that RKR curve yielded $\overline{\sigma}_f = 1.235$, which is distinctly worse than the agreement obtained from the DPF or unconstrained parameter fit. Moreover, even had the quality of the predictions been essentially equivalent, a pointwise RKR potential whose turning points must be interpolated over and extrapolated beyond is a distinctly less convenient way to describe the system than our analytical MLJ potential, which is valid at all distances. In addition, while Born–Oppenheimer breakdown corrections are expected to be relatively small for a large-reduced-mass system such as Rb_2, this will not be true, in general, and the conventional constrained-CDC parameter-fit approach cannot distinguish between adiabatic and nonadiabatic corrections to rotational energies, while the DPF method can.[16]

Our final comment draws attention to two slightly unsatisfactory features of the present direct fits to the MLJ potential. These are (1) the need to include a switching function in the exponent expansion to ensure that the MLJ potential exponent function does not have spurious unphysical behavior in the interval between the region governed by the experimental data and the asymptotic value defined by the theoretically known C_6 constant, and (2) the associated need to perform a manual search to determine α_S and R_S values that ensure the ''most reasonable'' behavior there. Unfortunately, we have not devised a solution to these deficiencies. The fact that the MLJ potential form incorporates the correct inverse-power asymptotic behavior does make it much more appropriate than most of the other potential models introduced in recent years.[40,41] However, the somewhat unsatisfactory nature of this manual search requirement should spur efforts to develop even more effective potential function models.

ACKNOWLEDGMENTS

We are pleased to thank Professor P. F. Bernath for helpful comments on the manuscript. This research was supported by the Natural Sciences and Engineering Research Council of Canada.

[1] C. Amiot, J. Chem. Phys. **93**, 8591 (1990).
[2] M. Anderson, J. R. Ensher, M. R. Matthews, C. E. Wieman, and E. A. Cornell, Science **269**, 198 (1995).
[3] C. C. Tsai, R. S. Freeland, J. M. Vogels, H. M. J. M. Boesten, B. J. Verhaar, and D. J. Heinzen, Phys. Rev. Lett. **79**, 1245 (1997).
[4] J. M. Vogels, C. C. Tsai, R. S. Freeland, S. J. J. M. F. Kokkelmans, B. J. Verhaar, and D. Heinzen, Phys. Rev. A **56**, R1067 (1997).
[5] H. M. J. M. Boesten, A. J. Moerdijk, and B. J. Verhaar, Phys. Rev. A **54**, R29 (1996).
[6] J. P. Burke, Jr., J. L. Bohn, B. D. Esry, and C. H. Greene, Phys. Rev. Lett. **80**, 2097 (1998).
[7] J. P. Burke, Jr. and J. L. Bohn, Phys. Rev. A **59**, 1303 (1999).
[8] C. Gabbanini, A. Fioretti, A. Lucchesini, S. Gozzini, and M. Mazzoni, Phys. Rev. Lett. **84**, 2814 (2000).
[9] (a) J. M. Hutson, J. Phys. B **14**, 851 (1981); (b) J. M. Hutson, QCPE Bulletin, 2, No. 2, Program #435, Quantum Chemistry Program Exchange, Indiana University, Bloomington, Indiana.
[10] A. N. Nesmeyanov, *Vapor Pressure of the Chemical Elements* (Elsevier, New York, 1963).
[11] C. E. Fellows, C. Amiot, and J. Vergès, J. Chem. Phys. **93**, 6281 (1990).
[12] C. E. Fellows, R. F. Gutterres, A. P. C. Campos, J. Vergès, and C. Amiot, J. Mol. Spectrosc. **197**, 19 (1999).
[13] See EPAPS Document No. E-JCPSA6-113-019032 for ASCII files containing listings of the data used and of all the fitted parameters yielded by the present work. This document may be retrieved via the EPAPS homepage (http://www.aip.org/pubservs/epaps.html) or from ftp.aip.org in the directory /epaps/. See the EPAPS homepage for more information.
[14] R. J. Le Roy, J. Mol. Spectrosc. **191**, 223 (1998).
[15] G. Audi and A. H. Wapstra, Nucl. Phys. A **565**, 1 (1993).
[16] R. J. Le Roy, J. Mol. Spectrosc. **194**, 189 (1999).
[17] A. H. M. Ross, R. S. Eng, and H. Kildal, Opt. Commun. **12**, 433 (1974).
[18] P. R. Bunker, J. Mol. Spectrosc. **68**, 367 (1977).
[19] J. K. G. Watson, J. Mol. Spectrosc. **80**, 411 (1980).
[20] R. J. Le Roy, *DSParFit 1.0. A Computer Program for Fitting Multi-Isotopomer Diatomic Molecule Spectra*, University of Waterloo Chemical Physics Research Report CP-646, 2000. The source code and manual for this program may be obtained from the www site http://theochem.uwaterloo.ca/~leroy.
[21] J. L. Dunham, Phys. Rev. **41**, 721 (1932).
[22] S. Z. Moody and C. L. Beckel, Int. J. Quantum Chem., Symp. **3**, 469 (1970).
[23] D. L. Albritton, W. J. Harrop, A. L. Schmeltekopf, and R. N. Zare, J. Mol. Spectrosc. **46**, 25 (1973).
[24] J. Tellinghuisen, Chem. Phys. Lett. **18**, 544 (1973).
[25] J. D. Brown, G. Burns, and R. J. Le Roy, Can. J. Phys. **51**, 1664 (1973).
[26] (a) R. Rydberg, Z. Phys. **73**, 376 (1931); (b) O. Klein, *ibid.* **76**, 226 (1932); (c) R. Rydberg, *ibid.* **80**, 514 (1933); (d) A. L. G. Rees, Proc. Phys. Soc. London **59**, 998 (1947).
[27] R. J. Le Roy, *LEVEL 7.0. A Computer Program Solving the Radial Schrödinger Equation for Bound and Quasibound Levels*, University of Waterloo Chemical Physics Research Report CP-642, 2000. The source code and manual for this program may be obtained from the www site http://theochem.uwaterloo.ca/~leroy.
[28] R. J. Le Roy, *RKR1. A Computer Program Implementing the First-Order RKR Method for Determining Diatom Potential Energy Curves from Spectroscopic Constants*, University of Waterloo Chemical Physics Research Report CP-425, 1992. The source code and manual for this program may be obtained from the www site http://theochem.uwaterloo.ca/~leroy.
[29] D. L. Albritton, W. J. Harrop, A. L. Schmeltekopf, and R. N. Zare, J. Mol. Spectrosc. **46**, 89 (1973).
[30] J. M. Hutson, S. Gerstenkorn, P. Luc, and J. Sinzelle, J. Mol. Spectrosc. **96**, 266 (1982).
[31] D. R. T. Appadoo, R. J. Le Roy, P. F. Bernath *et al.*, J. Chem. Phys. **104**, 903 (1996).
[32] A more sophisticated truncation procedure that cuts off the J, range at different points for different vibrational levels could also have been implemented here (Ref. 1), but it would not have changed this conclusion.
[33] C. Boone, ''Magnetic rotation in the $A\,^3\Pi_{1u} - X\,^1\Sigma_g^+$ system of $^{79}Br_2$,'' Ph.D. thesis, Department of Physics, University of British Columbia, 1999.
[34] R. J. Le Roy, Can. J. Phys. **52**, 246 (1974).
[35] W. M. Kosman and J. Hinze, J. Mol. Spectrosc. **56**, 93 (1975).
[36] C. R. Vidal and H. Scheingraber, J. Mol. Spectrosc. **65**, 46 (1977).
[37] J. A. Coxon, J. Mol. Spectrosc. **117**, 361 (1986).
[38] M. Gruebele, Mol. Phys. **69**, 475 (1990).
[39] R. Brühl, J. Kapetanakis, and D. Zimmermann, J. Chem. Phys. **94**, 5865 (1991).
[40] J. A. Coxon and P. G. Hajigeorgiou, J. Mol. Spectrosc. **150**, 1 (1991).
[41] H. G. Hedderich, M. Dulick, and P. F. Bernath, J. Chem. Phys. **99**, 8363 (1993).
[42] J. Tellinghuisen, J. Mol. Spectrosc. **173**, 223 (1995).
[43] A. Šurkus, Chem. Phys. Lett. **279**, 236 (1997).
[44] J. Y. Seto, Z. Morbi, F. Charron, S. K. Lee, P. F. Bernath, and R. J. Le Roy, J. Chem. Phys. **110**, 11 756 (1999).
[45] P. G. Hajigeorgiou and R. J. Le Roy, J. Chem. Phys. **112**, 3949 (2000).
[46] J. O. Hirschfelder, C. F. Curtiss, and R. B. Bird, *Molecular Theory of Gases and Liquids* (Wiley, New York, 1964).
[47] J. O. Hirschfelder and W. J. Meath, in *Intermolecular Forces*, Vol. 12 of Advances Chemical Physics, edited by J. O. Hirschfelder (Interscience, New York, 1967), pp. 3–106.
[48] R. J. Le Roy and R. B. Bernstein, J. Chem. Phys. **52**, 3869 (1970).
[49] J. Y. Seto, Direct fitting of analytic potential functions to diatomic molecule spectroscopic data, M.Sc. thesis, Department of Chemistry, University of Waterloo, 2000.
[50] A. Derevianko, W. R. Johnson, M. S. Safronova, and J. F. Babb, Phys. Rev. Lett. **82**, 3589 (1999).

[51] J. A. Coxon and P. G. Hajigeorgiou, J. Mol. Spectrosc. **193**, 306 (1999).
[52] (a) R. J. Le Roy and R. B. Bernstein, Chem. Phys. Lett. **5**, 42 (1970); (b) R. J. Le Roy and R. B. Bernstein, J. Chem. Phys. **52**, 3869 (1970).
[53] R. J. Le Roy, J. Chem. Phys. **73**, 6003 (1980).
[54] R. J. Le Roy and W.-H. Lam, Chem. Phys. Lett. **71**, 544 (1980).
[55] R. J. Le Roy, J. Chem. Phys. **101**, 10 217 (1994).
[56] R. J. Le Roy, *GvNDE. A Computer Program for Performing ''Near-Dissociation-Expansion'' Fits to Diatomic Molecule Vibrational Energies*. The source code for this program may be obtained by sending a request by e-mail to the author at ''leroy@UWaterloo.ca.''
[57] M. Marinescu, H. R. Sadeghpour, and A. Dalgarno, Phys. Rev. A **49**, 982 (1994).